

Theoretical Aspects of Chemical Reactivity
A. Toro-Labbé
© 2006 Elsevier B.V. All rights reserved.

Chapter 6

Electronic structure and reactivity in double Rydberg anions: characterization of a novel kind of electron pair

Junia Melin, Gustavo Seabra, and J. V. Ortiz

Department of Chemistry, Kansas State University, Manhattan, KS 66506-3701, USA

Abstract

A double Rydberg anion (DRA) consists of a stable cationic core and two electrons in a diffuse Rydberg orbital. These anions correspond to a local minimum on a potential energy surface where more stable isomers may exist. Experimental and theoretical works have contributed to a better understanding of the unusual electronic structure of these molecules. With electron propagator calculations and analysis of the electron localization function, some relationships between electronic structure and reactivity in DRAs are considered.

1. Introduction

In a pioneering photoelectron study of the anion–molecule complex H^-NH_3 , workers at Johns Hopkins University discovered a low-energy peak that could not be assigned to a hot band of this anion–molecule complex.¹ The invariance of the latter peak's position with respect to deuteration, which eliminated hot bands of the anion–molecule complex from consideration, led these workers to propose the presence of another isomer in the mass-selected ion sample. They subsequently proposed that this feature pertained to a tetrahedral NH_4^- anion.² Perturbative electron propagator calculations provided an accurate assignment of the photoelectron spectrum, ascribing the two principal peaks to a H^-NH_3 complex and the low-energy peak to a tetrahedral anion.³ The Dyson orbital corresponding to the latter feature has a_1 symmetry and exhibits NH antibonding and

HH bonding relationships between diffuse s functions. Such phase relationships and the predominance of diffuse s functions on hydrogens explained the sharpness of the corresponding photoelectron peak. This description also validated the use of the term double Rydberg anion (DRA),^{2,4} for two electrons are found in a Rydberg-like orbital that is distributed on the periphery of a closed-shell cation, NH_4^+ .

Several theoretical works were published on other simple hydrides and, in addition to tetrahedral NH_4^- DRAs have been found⁵⁻¹³ for C_{3v} OH_3^- and tetrahedral PH_4^- . Geometry optimizations of C_{3v} SH_3^- and linear structures of FH_2^- and ClH_2^- encountered transition states (TS) instead of DRA minima.¹⁰ The same study provided harmonic vibrational frequencies for NH_4^- , OH_3^- , and PH_4^- .

Recent calculations on NH_3R^- and OH_2R^- anions, where $\text{R} = \text{CH}_3, \text{NH}_2, \text{OH}$, and F , have identified other stable anions of this type.¹⁴ Here, AH_n substituents replace hydrogens from the parent species, tetrahedral NH_4^- , and C_{3v} OH_3^- . Dyson orbitals for electron detachments from stable anions such as NH_3CH_3^- are delocalized over the periphery of the entire species. This result extends previous studies where large molecular cations were found to accommodate a diffuse, Rydberg electron that is spread over the periphery of the entire cationic kernel.¹⁵ Covalent and ionic bonding that involves Rydberg-like orbitals has been explored as well.¹⁶

Experiments with higher resolution on N_2H_7^- ¹⁷ were quickly followed by electron propagator calculations¹⁸ that confirmed the existence of an anion-molecule complex, $\text{H}^-(\text{NH}_3)_2$, and two DRAs with vertical electron-detachment energies placed symmetrically about the position of the low-energy peak in the NH_4^- spectrum. One of these N_2H_7^- species is a complex consisting of the tetrahedral DRA and a coordinated ammonia molecule. The other features a hydrogen bond between two N atoms in a structure that resembles the $\text{N}_2\text{H}_7^+(\text{NH}_4^+ - \text{NH}_3)$ complex. The Dyson orbital for anion electron detachment in the latter isomer is localized on the three nonbridging hydrogens attached to the ammonium fragment's N atom. Vibrational satellites of each of the three vertical peaks also were assigned. Agreement of equally high quality was obtained for vibrational satellites seen in the NH_4^- spectrum.

These works established the existence of a novel variety of electron pair in DRAs.

Extensions of traditional electron pair concepts are clearly needed for these anions. The electron localization function (ELF)¹⁹ is an interesting and robust descriptor of chemical bonding, which has been successfully applied to a wide variety of molecular systems.²⁰⁻²⁴ This function, which is based on a topological analysis of a quantum function related to Pauli repulsion, describes the degree of localization (or delocalization) of electron pairs within the molecular space.

Section 2 explains the theory behind electron propagator calculations and the ELF. Section 3.1. contains results of ELF analysis for NH_3R^- DRAs (with $\text{R} = \text{H}, \text{CH}_3, \text{NH}_2, \text{OH}$) and molecular complexes of N_2H_7^- . After validation of the topological ELF analysis in the characterization of Rydberg electrons, the next step (described in Section 3.2.) is to study the reaction path that connects a DRA with a global minimum in the corresponding potential energy surface. In particular, we studied the reaction profile between tetrahedral NH_4^- and the H^-NH_3 complex. Our goal is to find the TS and determine the activation energy for this reaction. Through electronic structure calculations at different geometries along the energy profile, we expect to find when the double Rydberg character of NH_4^- is lost in favor of electronic distributions that are characteristic of ion-molecule complexes.

2. Theory

2.1. Electron propagator theory

Electron propagator calculations^{25–28} of electron-binding energies (that is, electron-attachment and -detachment energies) may be based on one-electron equations which read

$$\left[F + \Sigma \left(\varepsilon_i^{\text{Dyson}} \right) \right] \phi_i^{\text{Dyson}} = \varepsilon_i^{\text{Dyson}} \phi_i^{\text{Dyson}} \quad (1)$$

where F , the Fock operator, depends on the first-order density matrix of a reference state, $\Sigma(\varepsilon)$ is the energy-dependent, nonlocal correlation operator known as the self-energy, $\varepsilon_i^{\text{Dyson}}$ is a self-consistent eigenvalue and ϕ_i^{Dyson} is the corresponding eigenfunction known as the Dyson orbital. The eigenvalues equal electron-binding energies, and the Dyson orbitals are defined by the following equations for electron-detachment energies

$$\begin{aligned} \phi_i^{\text{Dyson}}(x_1) &= \sqrt{N} \int \Psi_N(x_1, x_2, x_3, \dots, x_N) \\ &\quad \times \Psi_{i,N-1}^*(x_2, x_3, \dots, x_N) dx_2 dx_3 \dots dx_N \end{aligned} \quad (2)$$

and electron-attachment energies

$$\begin{aligned} \phi_i^{\text{Dyson}}(x_1) &= \sqrt{N+1} \int \Psi_{i,N+1}(x_1, x_2, x_3, \dots, x_{N+1}) \\ &\quad \times \Psi_N^*(x_2, x_3, \dots, x_{N+1}) dx_2 dx_3 \dots dx_{N+1} \end{aligned} \quad (3)$$

where x_j is the space-spin coordinate of electron j , Ψ_N is an initial state with N electrons and $\Psi_{i,N\pm 1}$ is the i -th final state with $N \pm 1$ electrons. Diagonal approximations neglect off-diagonal matrix elements of the self-energy operator in the canonical, Hartree–Fock (HF) basis. Perturbative arguments underlie the second order, third order, P3 and OVGf diagonal approximations of the self-energy operator. The more advanced Brueckner Doubles T1 (BD-T1) method²⁵ does not make the diagonal approximation and includes partial, infinite-order contributions to the self-energy operator. The latter corrections are generated by the use of the Brueckner Doubles coupled-cluster wave function to describe the initial state and by other techniques, which consider final-state orbital relaxation and differential correlation effects. The norm of the Dyson orbital, p_i , reads

$$p_i = \int |\phi_i^{\text{Dyson}}(x_1)|^2 dx_1 \quad (4)$$

and is an index of the qualitative validity of the perturbative arguments that are made in the diagonal approximations. In the latter methods, the Dyson orbital equals the square root of the pole strength times a canonical, HF orbital. In contrast, Dyson orbitals generated with nondiagonal methods are expressed as a linear combination of orbitals pertaining to the reference state, which may be of the HF or Brueckner varieties.

2.2. Electron localization function

The ELF function is defined according to

$$\eta(r) = \left[1 + \left[\frac{T(r)}{T_{\text{TF}}(r)} \right]^2 \right]^{-1} \quad (5)$$

and is interpreted as a local measure of Pauli repulsion.¹⁹ In this equation, $T(r)$ represents the difference between the kinetic energy density of the real system and the exact kinetic energy density of a fictitious bosonic system with the same electronic density. Therefore, $\eta(r)$ measures the degree of electron pairing with respect to a homogeneous electron gas whose kinetic energy density is given by the Thomas–Fermi model, $T_{\text{TF}}(r)$. ELF values are close to 1 for localized electron pairs, whereas small values of this function ($\eta(r) < 0.5$) correspond to highly delocalized electron density. The topological analysis of the ELF provides a useful partition of molecular space into subsystems, called basins. These nonoverlapping regions are categorized as either core or valence basins, where valence basins are labeled by the number of connections with core basins, or synaptic order. A monosynaptic basin, $V(X_1)$, typically describes lone pairs that belong to X_1 . A disynaptic basin, $V(X_1, X_2)$, describes bonds between X_1 and X_2 atomic centers. Basins associated with more than three atomic cores are called polysynaptic. Of greatest importance in the following discussion are the asynaptic basins, which describe electrons that are not connected with atomic centers.^{21,29} Basins provide not only a useful qualitative picture of the electron pairs in a molecule, but they also have well-defined properties.³⁰ For example, electron population of a given basin is obtained by integrating the electron density over its volume Ω_i ,

$$\tilde{N}_i = \int_{\Omega_i} \rho(r) dr \quad (6)$$

The relative fluctuation of these populations, λ , has been suggested as a measure of the degree of electron delocalization.³¹ It is defined as,

$$\lambda(\tilde{N}_i) = \frac{\sigma^2(\tilde{N}_i)}{\tilde{N}_i} \quad (7)$$

where $\sigma^2(\tilde{N}_i)$ is the variance or quantum uncertainty associated with \tilde{N}_i .

2.3. Methods of calculation

The following strategy for electronic structure calculations on DRAs was employed. Geometry optimization and harmonic frequency analysis for the cations were performed at the HF level with a standard Pople basis set.^{14,18} These structures were used as initial guesses in the optimization of the respective anions, where the 6-311 + G(d,p) basis set, which includes diffuse functions, was used. By this stage, optimizations and frequency calculations could be refined using a higher level of theory; therefore, MP2 and QCISD calculations were performed for all the molecular systems. The diffuse

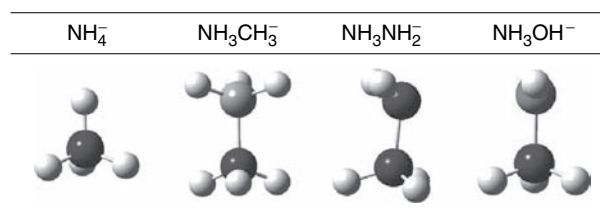


Figure 1 Optimized structures for NH_3R^- systems

nature of the highest occupied molecular orbital in the DRAs requires that the basis set be supplemented with an additional set of diffuse functions. Exponents for diffuse Gaussian functions were obtained by multiplying the smallest exponent with a given angular dependence by 1/3. In this manner, sp functions on nitrogen atoms and additional s functions on hydrogen were added. The ELF analysis was performed on the electron density obtained from single point calculations at the MP2 level with a bigger basis set, 6-311++G(2df,2p) augmented with extra diffuse functions, at the anion equilibrium geometries (see Fig. 1). Gaussian03³² was employed for all these calculations, whereas the ELF analysis was carried out with the TopMod³³ package of programs and Vis5d software³⁴ for visualization.

The TS for the internal conversion of the tetrahedral NH_4^- DRA into the $\text{H}^- \text{NH}_3$ complex was obtained at the MP2 level with the usual basis set treatment, and it was characterized by a unique imaginary frequency ($525i \text{ cm}^{-1}$). The reaction profile was obtained by performing an intrinsic reaction coordinate (IRC) calculation³⁵ upon the TS structure. Some points on this profile were chosen for a full analysis with electron propagator methods, including several diagonal self-energy approximations and the BD-T1 method.²⁵ Finally, topological analysis of the ELF was performed on various points along the reaction path.

3. Results and discussion

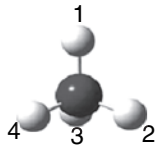
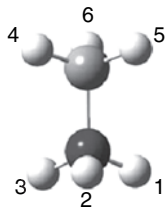
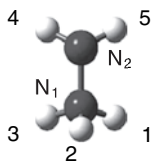
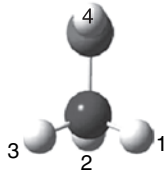
3.1. ELF analysis of DRA systems

In this section, ELF analysis for NH_3R^- systems (with $\text{R} = \text{H}, \text{CH}_3, \text{NH}_2, \text{OH}$) and molecular complexes of N_2H_7^- is presented. The color convention for all pictures is green for NH bonds, blue for lone pair electrons, and red for Rydberg electrons. Note that in some figures there are small red dots which correspond to core electrons. These features will be ignored in tables and in qualitative descriptions.

In general, all the systems analyzed with ELF function show asynaptic basins, which by definition are associated with none of the atomic cores in the molecule. Because Rydberg electrons and asynaptic basins are absent in the parent cations, asynaptic basins can be assigned to Rydberg electrons in the uncharged and anionic species. High fluctuation values found for these basins reflect a high degree of delocalization.

ELF results for NH_4^- in Table 1 show four equivalent bisynaptic basins corresponding to NH bonds, which are equivalent in tetrahedral symmetry. The electron population is about 2.0 electrons for each of them, and fluctuation values are in agreement with typical NH single bonds. Four asynaptic valence basins also are found. With a 0.24

Table 1

Molecule	Basin	N	σ^2	λ
	V(H1,N)	2.02	0.79	0.39
	V(H2,N)	2.02	0.79	0.39
	V(H3,N)	2.02	0.79	0.39
	V(H4,N)	2.02	0.79	0.39
	V(Asyn)	0.24	0.21	0.89
	V(Asyn)	0.24	0.21	0.89
	V(Asyn)	0.24	0.21	0.89
	V(H1,N)	2.07	0.82	0.4
	V(H2,N)	2.07	0.83	0.4
	V(H3,N)	2.07	0.82	0.4
	V(H4,C)	2.04	0.64	0.31
	V(H5,C)	2.04	0.64	0.31
	V(H6,C)	2.04	0.64	0.31
	V(N,C)	1.78	0.97	0.54
	V(Asyn)	0.46	0.36	0.78
	V(Asyn)	0.47	0.37	0.78
	V(Asyn)	0.46	0.36	0.78
	V(H1,N1)	2.08	0.79	0.38
	V(H2,N1)	2.11	0.81	0.38
	V(H3,N1)	2.08	0.8	0.38
	V(H4,N2)	2.01	0.79	0.39
	V(H5,N2)	2.01	0.78	0.39
	V(N1,N2)	1.54	0.91	0.59
	V(N2)	2.24	0.96	0.43
	V(Asyn)	1.03	0.55	0.54
	V(H1,N)	2.11	0.81	0.38
	V(H2,N)	2.14	0.81	0.38
	V(H3,N)	2.11	0.8	0.38
	V(H4,O)	1.7	0.81	0.48
	V(N,O)	1.19	0.79	0.66
	V(O)	2.38	1.07	0.45
	V(O)	2.42	1.08	0.45
	V(Asyn)	1.14	0.54	0.48
V(Asyn)	0.26	0.23	0.88	

electron population, these basins have a very high λ value: 0.89 on a scale of 0 to 1. Figure 2 shows the graphic representations of the ELF analysis for this anion. As has been mentioned above, the ELF function approaches unity for localized electron pairs. N core electrons and NH bonds can be identified clearly at $\eta(r) = 0.8$. Rydberg electrons are highly delocalized when $\eta(r) = 0.3$, and they are located preferentially close to hydrogen atoms (Fig. 2b). A spherical distribution of Rydberg basins around the cation core is observed even with a smaller isosurface where $\eta(r) = 0.20$. Figure 2c is in agreement with the analysis based on the Dyson orbital for electron detachment from the anion.¹⁸

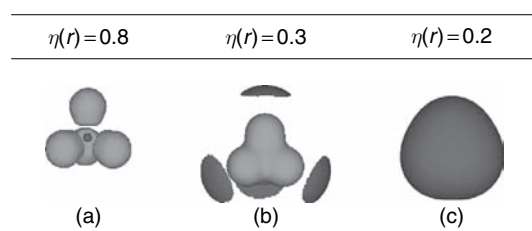
01
02
03
04
05
06
07
08
09
10
11
12
13
14
15
16
17
18
19
20
21
22
23
24
25
26
27
28
29
30
31
32
33
34
35
36
37
38
39
40
41
42
43
44
45
46
47

Figure 2 Topological analysis of ELF function for NH_4^+

For the NH_3CH_3^- anion, valence basins describing NH, CH, and NC bonds are found. Three asynaptic basins account for Rydberg electrons. The populations for these basins are slightly higher than their counterparts in the NH_4^+ anion, but λ values are smaller. Figure 3a depicts the ELF topology for this system at different isosurface values. Rydberg basins again are highly delocalized for $\eta(r) = 0.30$ and are located in regions close to H atoms belonging to the NH_3 fragment. At lower $\eta(r)$ values, Rydberg basins are expanded until they completely envelop the NH_3 portion of the anion.

In NH_3NH_2^- , a lone electron pair is present which reduces the symmetry of the system. ELF analysis shows three bisynaptic basins corresponding to NH bonds in the NH_3 fragment. Only two of them are equivalent in electron population, but all three have the same fluctuation value. There are two NH basins that belong to the NH_2 fragment and another bisynaptic region describing the NN bond. Rydberg electrons are contained in a unique asynaptic basin which contains only 1.03 electrons. The fluctuation value assigned to this basin is comparable with those of the NN and NC bonds. Figure 3b shows the corresponding pictures for this system. Rydberg electrons can be identified at $\eta(r) = 0.4$. Exploring the lowest values for the *ELF* isosurface, it is possible to see how Rydberg electron density encloses the anion and interacts even with the *H* atoms of the NH_2 substituent while leaving free the region around the lone pair.

The NH_3OH^- anion behaves similarly. NH bonds, with about the same electron populations and λ values as those of the previous cases, are found. Two monosynaptic

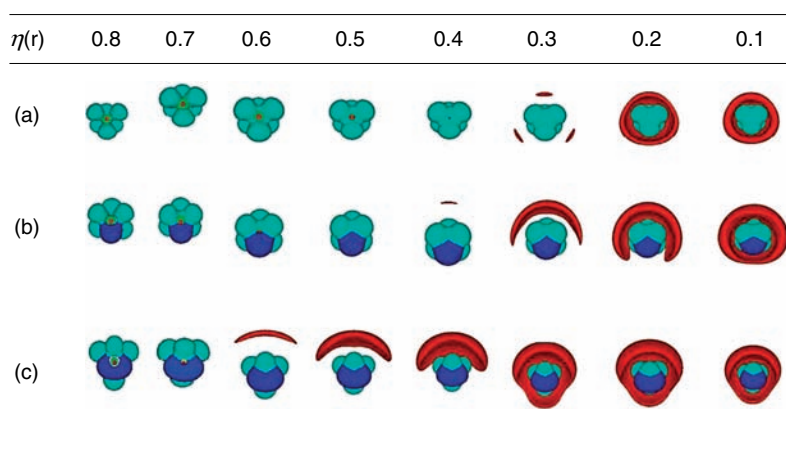


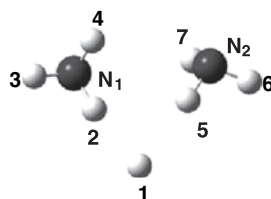
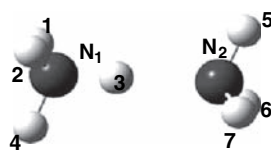
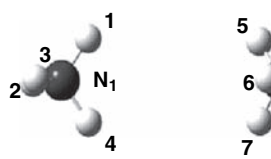
Figure 3 Topological analysis of ELF function for (a) NH_3CH_3^- , (b) NH_3NH_2^- , and (c) NH_3OH^-

basins describing lone pairs on the oxygen concentrate high electron population, but their fluctuations reveal delocalization. Rydberg electrons in this case are split into two basins. In Figure 3c, the Rydberg basin with larger population is located in the opposite direction with respect to the lone pairs and interacts with H₁ and H₃ of the NH₃ fragment. The remaining asymptotic basin, with a very small population and high delocalization, appears for $\eta(r) = 0.4 - 0.3$.

From a general point of view, Figure 3 shows the evolution of the isosurface value for the last three anionic systems. It is clear that the presence of lone pairs has an important effect on the Rydberg electrons' localization. Repulsions with lone pair electrons distort the Rydberg electrons toward the more positive regions of the anion.

Results for N₂H₇⁻ complexes are summarized in Table 2 and Figure 4. The most stable arrangement corresponds to two ammonia molecules coordinated to a hydride

Table 2

Complex	Basin	<i>N</i>	σ^2	λ
	V(H1)	2.83	0.90	0.32
	V(H2,N1)	1.48	0.90	0.60
	V(H3,N1)	1.90	0.76	0.40
	V(H4,N1)	1.89	0.75	0.40
	V(H5,N2)	1.48	0.90	0.61
	V(H6,N2)	1.90	0.75	0.40
	V(H7,N2)	1.89	0.76	0.40
	V(N1)	2.20	0.96	0.44
	V(N2)	2.20	0.96	0.44
		V(H1,N1)	2.05	0.84
V(H2,N1)		2.03	0.79	0.39
V(H3,N1)		1.97	0.78	0.39
V(H4,N1)		2.04	0.79	0.39
V(H5,N2)		2.01	0.80	0.40
V(H6,N2)		1.92	0.78	0.40
V(H7,N2)		1.96	0.79	0.40
V(N2)		2.09	1.00	0.48
V(Asyn)		0.34	0.29	0.84
V(Asyn)		0.35	0.29	0.84
V(Asyn)	0.32	0.28	0.85	
	V(H1,N1)	2.04	0.80	0.39
	V(H2,N1)	2.03	0.80	0.40
	V(H3,N1)	2.03	0.80	0.39
	V(H4,N1)	2.01	0.80	0.40
	V(H5,N2)	1.95	0.77	0.39
	V(H6,N2)	1.94	0.76	0.39
	V(H7,N2)	1.93	0.76	0.39
	V(N2)	2.14	0.95	0.45
	V(Asyn)	0.41	0.33	0.81
	V(Asyn)	0.37	0.31	0.83
V(Asyn)	0.24	0.21	0.89	
V(Asyn)	0.22	0.20	0.90	

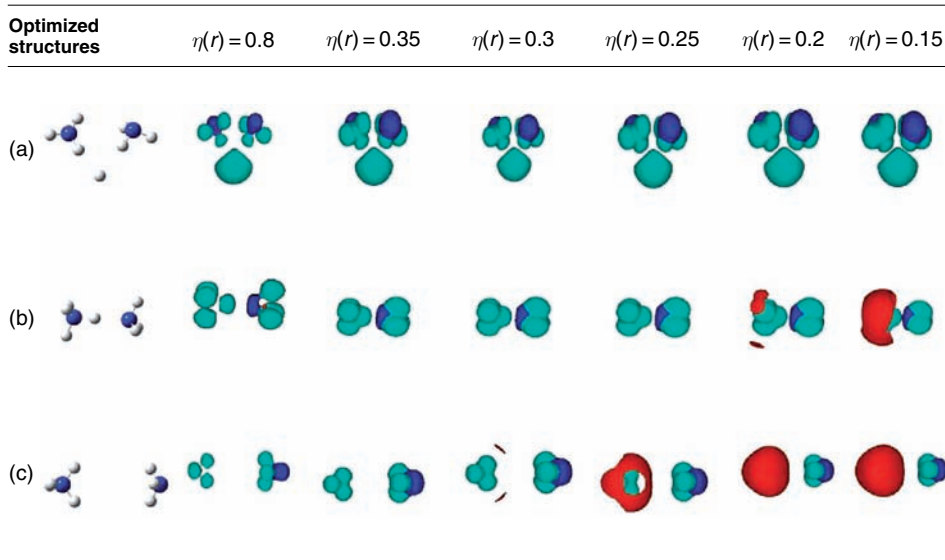


Figure 4 Topological analysis of ELF function for (a) $\text{H}^-(\text{NH}_3)_2$, (b) bridge, and (c) $\text{NH}_4^-(\text{NH}_3)$

(Fig. 4a). Topological analysis of this ionic structure does not find any asynaptic basin. Therefore, one may conclude that this complex has no Rydberg character. Another minimum that is less stable by 0.5 eV also was found. In this case, the NH_4^- anion is bridged to an ammonia molecule. Three Rydberg basins, with almost the same population and fluctuation, are present. The highly delocalized electrons of these basins can be visualized only when $\eta(r) = 0.2$ or less. Finally, a third structure exhibits coordination between NH_4^- and NH_3 fragments. Four asynaptic basins are present in this structure. Two of them, identified as occupying the region between the molecules, are almost equivalent in population and slightly more localized than the other two. The isosurfaces depicted in Figure 4c show how two Rydberg basins appear at $\eta(r) = 0.3$, whereas at $\eta(r) = 0.2$ the NH_4^- molecule is completely covered by Rydberg electron density. From the last picture, one can conclude that this complex corresponds to a NH_4^- DRA coordinated to an ammonia molecule.

3.2. Transformation of a DRA to an ion–molecule complex

Figure 5 shows the energy profile for the reaction. A sharp increase of energy is observed in the pathway from the reactant to the TS. Enlargement of the NH bond distance occurs with retention of C_{3v} symmetry. After the TS, energy decays slowly, but with more drastic geometry changes. The detached H_4 atom (see Table 3 for numbering) travels around the NH_3 fragment, leaving the C_{3v} axis soon after the TS. Table 3 summarizes the geometries for stationary points on this profile. The TS has geometrical parameters that resemble those of the tetrahedral form of NH_4^- , but with an obvious elongation between H_4 and the nitrogen atom. The final product is a complex between a hydride anion and an ammonia molecule. The latter species has NH bond lengths that are close to those of

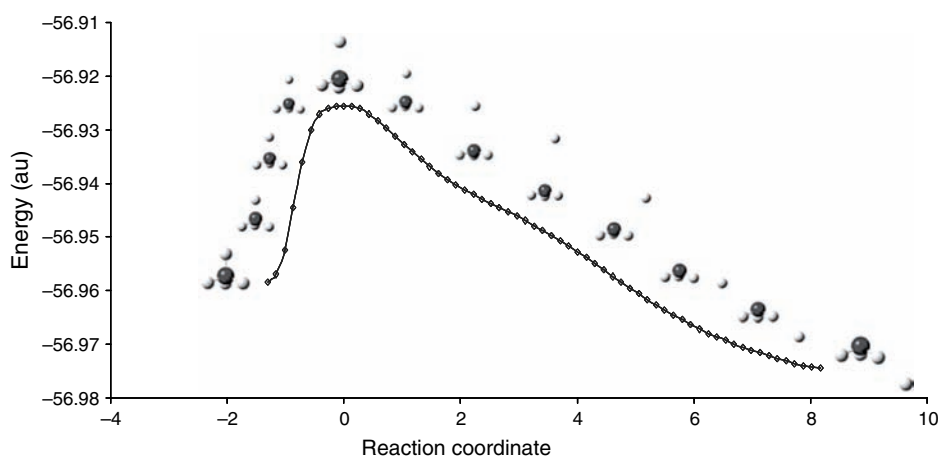
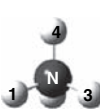
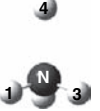
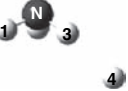


Figure 5 Reaction profile for internal conversion of NH_4^- DRA to $\text{H}^- \text{NH}_3$ complex with respect to an arbitrary reaction coordinate

Table 3 Geometrical parameters of reactant, transition state, and product

			
N-H ₂	1.0182	1.0218	1.0141
N-H ₄	1.0182	1.7501	2.8340
H ₁ -N-H ₂	109.47	108.73	103.97
H ₁ -N-H ₄	109.47	110.20	99.95
H ₄ -N-H ₁ -H ₂	120.00	120.88	-103.18

Distances in Å, angles in degrees.

an isolated NH_3 molecule, but with HNH angles that are smaller. The activation energy for this reaction, ΔE_{act} , has been determined to be 0.59 eV (13.58 kcal/mol), whereas the energy difference between reactant and product, ΔE_{R} , is -0.68 eV (-15.59 kcal/mol). These values include zero-point energy corrections.

Bowen's experimental work assigned an electron-detachment energy of 0.47 eV to the tetrahedral NH_4^- anion, whereas the main peak, corresponding to an electron-binding energy of the $\text{H}^- \text{NH}_3$ complex, was determined to be 1.11 eV. Table 4 lists vertical electron-detachment energies (VEDEs) calculated with different approximations of electron propagator theory for the reactant, the product and ten other molecular structures along the reaction path, including the TS. As has been discussed elsewhere, due to strong electron correlation in the DRA, Koopmans values do not agree closely with the experiment. Nevertheless, these values are included in the table as a comparative reference for an uncorrelated method. Propagator calculations within the diagonal self-energy approximation, namely, second and third order, OVGf and P3, provide better descriptions than HF orbital energies, but still do not give an accurate account of the

Table 4 Vertical electron-detachment energies (in eV), with different approximations, along the reaction path

	KT	2 nd	3 rd	OVGF	P3	BD-T1					
React	-0.229	-0.530	(0.898)	-0.435	(0.846)	-0.359	(0.754)	-0.459	(0.860)	-0.477	(0.856)
2	-0.242	-0.553	(0.893)	-0.436	(0.844)	-0.356	(0.759)	-0.481	(0.855)	-0.472	(0.859)
3	-0.282	-0.509	(0.848)	-0.316	(0.798)	-0.219	(0.717)	-0.408	(0.80)	-0.285	(0.796)
4	-0.358	0.002	(0.759)	-0.017	(0.714)	-0.021	(0.701)	0.10	(0.736)	-0.125	(0.686)
TS	-0.382	0.122	(0.752)	0.002	(0.718)	-0.023	(0.712)	0.187	(0.745)	-0.138	(0.677)
6	-0.410	0.223	(0.749)	0.001	(0.732)	-0.05	(0.727)	0.249	(0.759)	-0.159	(0.662)
7	-0.795	0.097	(0.805)	-0.311	(0.905)	-0.417	(0.893)	-0.01	(0.905)	-0.343	(0.747)
8	-0.953	-0.184	(0.832)	-0.428	(0.903)	-0.565	(0.895)	-0.214	(0.909)	-0.393	(0.755)
9	-1.170	-0.481	(0.850)	-0.634	(0.893)	-0.777	(0.890)	-0.454	(0.902)	-0.574	(0.796)
10	-1.411	-0.779	(0.862)	-0.881	(0.889)	-1.024	(0.888)	-0.712	(0.897)	-0.817	(0.813)
11	-1.563	-0.943	(0.868)	-1.064	(0.894)	-1.191	(0.893)	-0.883	(0.901)	-1.001	(0.828)
Prod	-1.629	-0.993	(0.870)	-1.165	(0.90)	-1.265	(0.899)	-0.968	(0.906)	-1.102	(0.793)

Pole strength values are in parentheses.

photoelectron spectrum. For instance, second order and P3 underestimate the VEDE of the H^-NH_3 complex, but third order and OVGF overestimate this transition energy. As for the reactant, second order predicts a higher VEDE, and the remaining methods are below the experimental value. A global inspection of these diagonal methods reveals how the electron-binding energy decreases from the reactant to the TS, reaching a negative value for the latter structure and its neighbors. The OVGF approximation is an exception, for it predicts a small but still positive VEDE at the TS. Pole strengths present interesting trends, for they are mostly around 0.85 in the reactant, decreasing quickly as the reaction evolves to the TS structure. Afterward these values increase again, until they reach 0.9 in the product. The definition of the pole strength parameter in propagator theory implies that when it is close to the unity, Koopmans's approximation is qualitatively valid. Therefore, the small values obtained around the TS reveal that the overlap between Dyson and occupied HF molecular orbitals is poor in this region, and a better electron correlation treatment is required. Note that the smallest pole strength is placed just before the TS and not on that point as might be expected. The reason for this finding is that the TS structure is no longer a DRA. This hypothesis will be supported in the following discussion of ELF results. Electron-detachment energies obtained with the BD reference state merit attention, since this method goes beyond the diagonal self-energy approach and has a more flexible treatment of correlation. For reactant and product, BD-T1 values show an excellent agreement with the experimental spectrum. Binding energies are small around the TS, but are all positive. The lowest ionization energy belongs to the structure previous to the TS, but the minimum value for the pole strength occurs afterward. The pole strength of the reactant is higher than that for the product.

Results of ELF topological analysis are depicted in Figure 6. For simplicity, not all of the calculated structures have been included, but the picture illustrates how the basin distribution varies along the reaction path. Because of the high delocalization of Rydberg electrons, the plots correspond to a small ELF value, $\eta(r) = 0.25$, in all cases. For the reactant, NH_4^- , four peripheral Rydberg basins around the cation core are found,

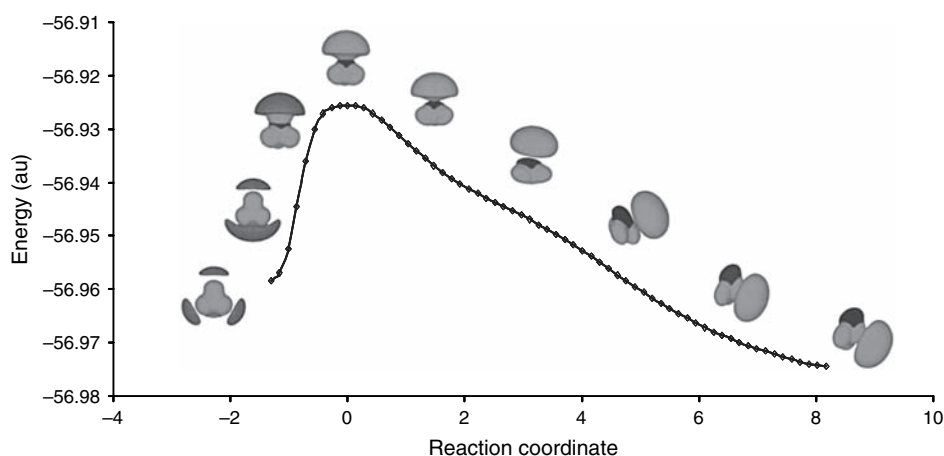


Figure 6 ELF analysis along the reaction profile for internal conversion of NH_4^- DRA to $\text{H}^- \text{NH}_3$ complex

just as has been described in previous section. The following structure shows just two red basins, where the Rydberg electrons are polarized along the C_{3v} axis. As the energy increases, Rydberg electrons are more localized on the leaving H atom and are found finally within a monosynaptic basin that corresponds to a hydride anion. At the TS structure, the asynaptic basins are gone and lone pair electrons on nitrogen appear in blue. The reaction has evolved to the product, where H^- and NH_3 fragments may be identified clearly.

4. Conclusions

The present study confirms the existence of a novel variety of electron pair. In contrast to the bonding pairs of Lewis and Langmuir and to the lone pairs of Moffitt, the diffuse electron pairs of NH_4^- and N_2H_7^- are built chiefly of extravalence atomic functions and occupy the periphery of molecular cations. The concept of a Rydberg electron pair may lead to the prediction or observation of similar species or it may eventually yield to more generalized qualitative concepts of electronic structure.

The reaction profile that is displayed in the figures demonstrates the presence of a considerable barrier to the rearrangement of NH_4^- from a tetrahedral, double Rydberg structure to an anion–molecule complex. In the TS, C_{3v} symmetry applies as one of the NH distances is markedly longer than the others. An additional reduction of symmetry occurs after the transition state with the formation of the hydride–ammonia complex.

Calculation of accurate electron-detachment energies along the entire reaction path requires the use of a highly correlated electron propagator approximation. Pole strengths associated with these transition energies have a minimum value near the transition state and indicate that correlation effects are largest at these geometries. Dyson orbitals for the electron-detachment energy also differ most from HF orbitals at these structures. The delocalized amplitudes of the Dyson orbital associated with the DRA have become more localized on the leaving hydrogen in the transition state.

01 Analysis of the electron localization function for geometries of the same reaction
02 path provides an alternative, but compatible, perspective on the evolution of electronic
03 structure. The novel asynaptic basin of the DRA, which represents a pair of electrons
04 that is delocalized over the periphery of the ammonium cation core, is transformed into
05 a conventional, monosynaptic basin that is associated with the departing hydrogen at
06 the geometries near the transition state. After the transition state, the NH_4^- system may
07 be described as a hydride–ammonia complex.

08 09 10 Acknowledgments

11 We acknowledge the support of the National Science Foundation through grant CHE-
12 0135823 to Kansas State University.

13 14 15 References

- 16 1. J. V. Coe, J. T. Snodgrass, C. B. Freidhoff, K. M. McHugh and K. H. Bowen, *J. Chem. Phys.*
17 **83**, 3169, (1985).
- 18 2. J. T. Snodgrass, J. V. Coe, C. B. Freidhoff, K. M. McHugh and K. H. Bowen, *Faraday Disc.*
19 *Chem. Soc.*, **86**, 241, (1988).
- 20 3. J. V. Ortiz, *J. Chem. Phys.* **87**, 3557, (1987).
- 21 4. J. Simons and M. Gutowski, *Chem. Rev.*, **91**, 669, (1991).
- 22 5. H. Cardy, C. Larrieu and A. Dargelos, *Chem. Phys. Lett.*, **131**, 507, (1986).
- 23 6. D. Cremer and E. Kraka, *J. Phys. Chem.*, **90**, 33, (1986).
- 24 7. M. Gutowski, J. Simons, R. Hernandez and H. L. Taylor, *J. Phys. Chem.*, **92**, 6179, (1988).
- 25 8. M. Gutowski and J. Simons, *J. Chem. Phys.*, **93**, 3874, (1990).
- 26 9. J. V. Ortiz, *J. Chem. Phys.*, **91**, 7024, (1989).
- 27 10. J. V. Ortiz, *J. Phys. Chem.*, **94**, 4762, (1990).
- 28 11. N. Matsunaga and M. S. Gordon, *J. Phys. Chem.*, Vol. 99, 12773, (1995).
- 29 12. J. Moc and K. Morokuma, *Inorg. Chem.*, **33**, 551, (1994).
- 30 13. G. Trinquier, J. P. Daudey, G. Caruana and Y. Madaule, *J. Am. Chem. Soc.*, **106**, 4794,
31 (1984).
- 32 14. H. Hopper, M. Lococo, O. Dolgounitcheva, V. G. Zakrzewski and J. V. Ortiz, *J. Am. Chem.*
33 *Soc.*, **122**, 12813, (2000).
- 34 15. A. I. Boldyrev and J. Simons, *J. Chem. Phys.*, **97**, 6621, (1992).
- 35 16. (a) A. I. Boldyrev and J. Simons, *J. Phys. Chem.*, **96**, 8840, (1992). (b) J. S. Wright and
36 D. McKay, *J. Phys. Chem.*, **100**, 7392, (1996). (c) A. I. Boldyrev and J. Simons, *J. Phys.*
37 *Chem. A*, **103**, 3575, (1999).
- 38 17. S. J. Xu, J. M. Niles, J. H. Hendricks, S. A. Lyapustina and K. H. Bowen, *J. Chem. Phys.*,
39 **117**, 5742, (2002).
- 40 18. J. V. Ortiz, *J. Chem. Phys.*, **117**, 5748, (2002).
- 41 19. A. D. Becke and K. E. Edgecombe, *J. Chem. Phys.*, **92**, 5397, (1990).
- 42 20. A. Savin, A. D. Becke, J. Flad, R. Nesper, H. Preuss and H. Von Schnering, *Angew. Chem.*
43 *Int. Ed. Engl.*, **30**, 409, (1991).
- 44 21. A. Savin, O. Jepsen, J. Flad, R. Nesper, O. K. Andersen, H. Preuss and H. G. Von Schnering,
45 *Angew. Chem.*, **31**, 187, (1992).
- 46 22. E. Chamorro, J. C. Santos, B. Gomez, R. Contreras and P. Fuentealba, *J. Chem. Phys.*, **114**,
47 23, (2001)
23. P. Fuentealba and A. Savin, *J. Chem. Phys. A*, **105**, 11531, (2001).

- 01 24. J. Melin and P. Fuentealba, *Int. J. Quant. Chem.*, **92**, 381, (2003).
02 25. J. V. Ortiz, *Adv. Quant. Chem.*, **33**, 35, (1999).
03 26. A. M. Ferreira, G. Seabra, O. Dolgounitcheva, V. G. Zakrzewski and J. V. Ortiz, in *Quantum*
04 *Mechanic Predictions of Thermochemistry Data*” edited by J. Cioslowski (Kluwer, Dordrecht,
05 2001), p. 131.
06 27. J. Linderberg and Y. Öhrn, in *Propagators in Quantum Chemistry*, Second Edition (Wiley,
07 Hoboken, New Jersey, 2004).
08 28. J. V. Ortiz, in *Computational Chemistry: Reviews of Quantum Current Trends, Vol 2*, edited
09 by J. Leszczynski (World Scientific, Singapore, 1997), p. 1.
10 29. A. Savin, B. Silvi and F. Colonna, *Can. J. Chem.*, **30**, 1088, (1996).
11 30. B. Silvi and A. Savin, *Nature*, **371**, 683, (1997).
12 31. R. F. W. Bader, in *Localization and Delocalization in Quantum Chemistry*, edited by O.
13 Chavet *et al.* (Riedel, Dordrecht, 1976)
14 32. Gaussian 03, Revision B.03, M. J. Frisch, G. W. Trucks, H. Schlegel, G. E. Scuseria,
15 M. A. Robb, J. R. Cheeseman, Jr., J. A. Montgomery, T. Vreven, K. N. Kudin, J. C. Burant, J.
16 M. Millam, S. S. Iyengar, J. Tomasi, V. Barone, B. Mennucci, M. Cossi, G. Scalmani, N. Rega,
17 G. A. Petersson, H. Nakatsuji, M. Hada, M. Ehara, K. Toyota, R. Fukuda, J. Hasegawa, M.
18 Ishida, T. Nakajima, Y. Honda, O. Kitao, H. Nakai, M. Klene, X. Li, J. E. Knox, H. P.
19 Hratchian, J. B. Cross, C. Adamo, J. Jaramillo, R. Gomperts, R. E. Stratmann, O. Yazyev, A. J.
20 Austin, R. Cammi, C. Pomelli, J. W. Ochterski, P.Y. Ayala, K. Morokuma, G. A. Voth, P.
21 Salvador, J. J. Dannenberg, V. G. Zakrzewski, S. Dapprich, A. D. Daniels, M. C. Strain, O.
22 Farkas, D. K. Malick, A. D. Rabuck, K. Raghavachari, J. B. Foresman, J. V. Ortiz, Q.
23 Cui, A. G. Baboul, S. Clifford, J. Cioslowski, B. B. Stefanov, G. Liu, A. Liashenko, P.
24 Piskorz, I. Komaromi, R. L. Martin, D. J. Fox, T. Keith, M. A. Al-Laham, C. Y. Peng, A.
25 Nanayakkara, M. Challacombe, P. M. W. Gill, B. Johnson, W. Chen, M. W. Wong, C.
26 Gonzalez, J. A. Pople, Gaussian, Inc., Pittsburgh PA, 2003.
27 33. S. Noury, X. Krokisdis, F. Fuster and B. Silvi, *Comput. Chem. Oxford.*, **23**, 597, (1999)
28 34. B. Hibbard, J. Kellum and B. Paul, vis 5d, version 5.2: Visualization Project, University of
29 Wisconsin-Madison Space Science and Engineering Center, 1990.
30 35. C. Gonzalez and H. B. Schlegel, *J. Chem. Phys.*, **90**, 2154, (1989) and *J. Chem. Phys.*, **94**,
31 5523, (1990).
32
33
34
35
36
37
38
39
40
41
42
43
44
45
46
47